annalen der physik
www.ann-phys.org

3D Optical Vortex Lattices

*Denis A. Ikonnikov, Sergey A. Myslivets, Vasily G. Arkhipkin, and Andrey M. Vyunishev**

Fresnel diffraction of light beams with a topological charge on a 2D regular amplitude transparency mask is studied. Numerical predictions show that the 3D optical lattices of optical vortices can be formed using the Talbot effect, with these predictions confirmed by the experimental reconstruction of all 3D optical vortex lattices. The periodicity of the 3D optical vortex lattices is determined by the light wavelength and periodicity of a transparency mask. Furthermore, it is shown that the optical vortices are created and annihilated during light propagation behind the mask with the preservation of the total topological charge. The 3D optical vortex lattices are considered to be tolerant to the perturbations induced by trapped particles caused by the features of the Talbot effect. The 3D optical vortex lattices open new possibilities for light–matter interactions and the related applications.

1. Introduction

Structured light, that is, the light with the complex intensity, phase, and polarization distributions, is an exciting object of study in photonics due to its extraordinary characteristics.[1,2] A bright example of structured light is an optical vortex (OV), which represents the light with an azimuthal phase dependence of $\exp(il\phi)$, where l is the topological charge (TC) and ϕ is the azimuthal angle.[3] The light with such phase dependences is characterized by the phase singularities with zero intensity. This makes the OVs highly desired for optical tweezers[4] due to the high intensity gradient around these singularities and makes it possible to overcome the diffraction limit and achieve the super-resolution.[5] The superposition of two OVs can result in the formation of bottle beams,[6] which are the light beams with a finite axial region of the near-zero intensity surrounded by the high-intensity light in all dimensions.[7] They are promising for 3D optical trapping of absorbing particles, which are trapped at the center of a bottle beam, where the thermal damage becomes negligible.[8,9] In addition, the orbital angular momentum (OAM) related to the OVs provides an additional degree of freedom for multiplexing, which results in the superior capacity of optical communication systems.[10,11] Of great interest are the spatial OV arrays. They are promising for a wide application range, including micromachining and structuring, trapping, sorting, and micromanipulation.[12–16] Single photons prepared in the OV lattice can inspire many fields of quantum optics.[17] The OV arrays can be created by multibeam interference,[18,19] diffraction on Damman gratings,[20] or using the Talbot effect.[21] Besides, in ref. [22] it was proposed a method for producing a close-packed 2D OV lattice with a controllable structure in the far-field. So far, the investigations of the OV arrays have been limited to the cross sections of the 3D spatial distributions,[21,23] except for the 3D reconstruction of a unit cell,[18,24] although 3D optical lattices without TCs have been intensively studied.[9,25] A spatial array of the OVs regular in the three dimensions (a 3D lattice) is of particular interest, since it offers unique possibilities for light-matter interactions, which cannot be obtained using optical lattices without TCs.

In this paper, Fresnel diffraction of light beams with a TC on a 2D regular amplitude transparency mask (diffraction grating) is examined. This approach is shown to be a straightforward and simple way to produce 3D OV lattices (OVLs).

2. Basic Theory

When a plane wave passes through a periodic grating, the near-field interference of the diffracted waves leads to the self-reproduction of the intensity distribution (image) at distances multiple of the Talbot length $Z_T = 2\Lambda^2/\lambda$, where Λ is the grating period and λ is the wavelength of the incident wave. This effect is well-known as the Talbot effect[26]; it has been shown that this effect is retained for OVs in the visible[24] and terahertz ranges.[21,23] It means that the Talbot effect can be used to create the 3D OVLs by illuminating a 2D amplitude diffraction grating with an OV as shown in **Figure 1**a. The 3D intensity distribution can be calculated using the approach proposed in ref. [24]. In the case of a squared regular grating, the light field diffracted behind the grating can be presented in the form

$$E(x,y,z) = i^{l-1}\left(-\frac{1}{2}\right)^{l}\frac{\pi w^{l+2}}{\lambda z(1-ia)^{l+1}} \times E_0 \exp\left[ikz + i(k/2z)(x^2+y^2)\right] \times \sum_{m,n} t_{mn}(b_{xm}+ib_{yn})^{l}\exp\left[-\frac{(b_{xm}^2+b_{yn}^2)w^2}{4(1-ia)}\right] \quad (1)$$

D. A. Ikonnikov, S. A. Myslivets, V. G. Arkhipkin, A. M. Vyunishev
Kirensky Institute of Physics
Federal Research Center KSC SB RAS
Krasnoyarsk 660036, Russia
E-mail: vyunishev@iph.krasn.ru
S. A. Myslivets, V. G. Arkhipkin
Institute of Engineering Physics and Radio Electronics
Siberian Federal University
Krasnoyarsk 660041, Russia

The ORCID identification number(s) for the author(s) of this article can be found under https://doi.org/10.1002/andp.202100114

DOI: 10.1002/andp.202100114

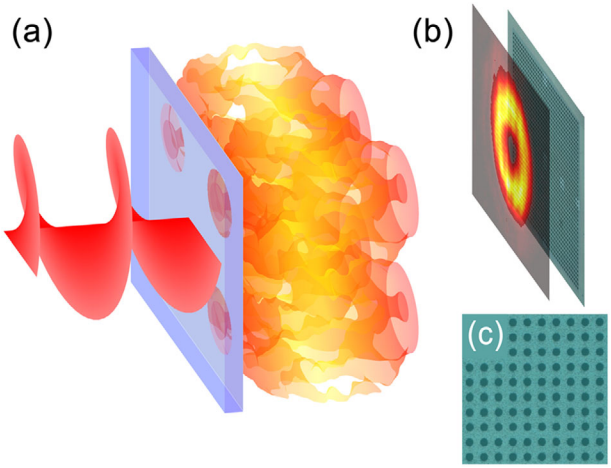

Figure 1. Schematic of the experiment: a) near-field diffraction of a helical wavefront wave on a 2D regular amplitude diffraction grating, b) measured profile of the OV beam ($l = +1$) incident on the grating, and c) SEM image of the grating.

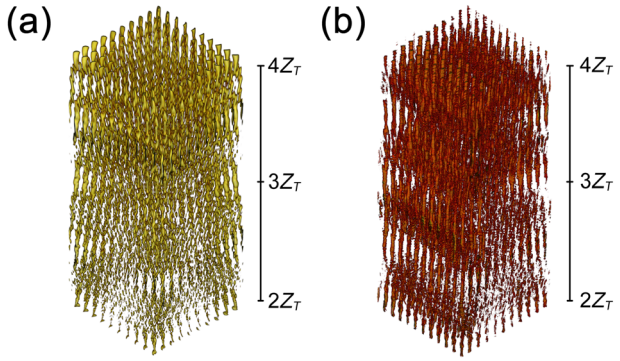

Figure 2. a) Calculated and b) experimental 3D optical vortex lattices with 10×10 periods and $z \in [2Z_T, 4Z_T]$ for $l = +1$.

Here, $b_{xm} = mG - (k/z)x$ and $b_{yn} = nG - (k/z)y$, $a = kw^2/2z$, k is the wavevector, w is the beam spot radius, $G = 2\pi/\Lambda$ is the reciprocal lattice vector, and the subscripts m, n are integers. The Fourier coefficients of the transmission function of the amplitude transparency grating $T(x_0, y_0)$ are

$$t_{mn} = \frac{1}{\Lambda^2} \iint_{-\Lambda/2}^{\Lambda/2} T(x_0, y_0) e^{[-iG(mx_0 + ny_0)]} dx_0 dy_0 \quad (2)$$

3. Results and Discussion

The calculated 3D OVL for 10×10 periods of the grating and the coordinate range $z \in [2Z_T, 4Z_T]$ is shown in **Figure 2**a. To obtain the best visualization of the 3D intensity distributions, the transparency was tuned such that the patterns were semitransparent at the intensity level below 0.8. At the Talbot planes (TP), the intensity pattern has good reproducibility and represents a set of vortices. At small distances (as far as the second Talbot plane), the intensity distribution is complex, which is quite expected and related to the diffraction features, since, in this region, the high-frequency spatial components make fairly a great contribution. Starting with the second Talbot plane, the intensity distribution becomes better ordered. Although the vortices become broader with increasing distance (during the propagation), they start overlapping from a certain point. Since the vortices with the higher TC are broader, they start overlapping at smaller distances.

In the experiments, a phase mask with the azimuthal phase modulation generated by a 2D phase-only spatial light modulator (SLM, PLUTO-NIR-011, Holoeye, a pixel pitch of 8 μm) was imposed on a Gaussian beam of a He–Ne laser (FWHM 546 μm) to obtain OVs (Figure 1b). The linearly polarized radiation with a wavelength of 632.8 nm was generated by a laser operated in a single-mode regime. To obtain the high-quality OVs, a fork-shaped hologram was loaded into the SLM, which provides the phase modulation in the form $\cos(G_x x + l\phi)$, where G_x is the reciprocal lattice vector. The OV beam was incident onto the structure in such a way that the OV center coincided with the center of the grating structure. The grating is a 2D regular array of round holes formed by ion etching on a Hitachi FB-2100 focused ion beam system from a transparent quartz plate coated with a silver film (Figure 1c). The grating periods were 10 μm and the hole diameter was about 5 μm. The overall size was 400×400 μm^2 with 40 periods along each axis. A beam profiler with a 100× objective was mounted on a translation stage behind the grating. An objective with the beam profiler moved along the translation stage with a step of 1 micron. At each step, the intensity profiles were recorded. A whole set of intensity profiles forms the 3D near-field intensity distribution. Thus, we obtained the experimental 3D OVLs for the parameters corresponding to the calculated ones, as shown in Figure 2b. To obtain the best agreement between the calculated and experimental 3D OVLs, the experimental intensity level below which the distribution became semitransparent was taken to 0.75. The discrepancy between this value and the calculated data is caused by the measurement error. Since the 3D distributions in Figure 2 are spatially periodic in each dimension, these 3D distributions can be treated as 3D optical lattices. The comparison of the calculated and experimental 3D OVLs showed that the periodicity along all the axes and shapes of individual beams are in good agreement.

Let us now consider Fresnel diffraction for different TCs of the incident beam. For more detailed analysis, we limit the consideration to the two periods of the 3D OVLs along both the x- and y- axes. It can be seen in **Figure 3** that the calculated and experimental 3D OVLs agree well, especially for low TCs. According to the rotational symmetry of the investigated configuration, the measurements were performed in the central low-intensity area of the incident beam, which made the analysis easier. Thus, it should be noted that the higher the TC, the broader the incident OV core, and the lower the intensity near the center. This leads to a decrease in both the signal-to-noise ratio and the image quality, while the fine structures within a unit cells become more complex with increasing TC. Unfortunately, the spatial resolution of the beam profiler was not enough to resolve fine structures for high TC values. As can be seen in Figure 3, the intensity maxima for TC $l = 0$ correspond to the positions of holes. This is drastically different from the case of TC $l \neq 0$. In the latter case, there are shadow regions related to the phase singularities (OVs) in these positions along the z-axis. As expected, during propagation of the beams along the z-axis, the intensity distribution became smooth. At the same

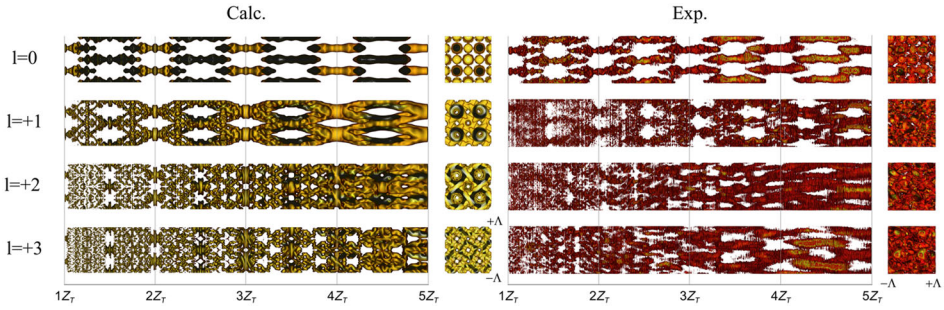

Figure 3. Side and front views of the calculated (the first and second columns) and experimental (the third and fourth columns) optical vortex lattices taken at $z \in [1Z_T, 5Z_T]$.

time, the vortices start overlapping at a certain point, thereby leading to the periodicity distortions. In contrast to the case of $l = 0$, the spatial structures of the 3D OVLs corresponding to TC $l \neq 0$ have no discontinuities at the considered intensity level.

Similar arrays of light, but without TCs, were previously investigated for optical trapping of particles, in particular, absorbing particles in a gaseous medium,[9] where the photophoretic forces dominate over the light pressure forces.[27] Thus, regardless of the refractive indices of a medium and particles, it is fair to say that absorbing particles will tend to move away from the areas with the maximum light intensity. In contrast, weakly absorbing ones will tend to occupy these areas. It should be noted, that in the beams with a nonzero TC, the intensity distributions are ring-like with the low intensity near the center, and in the optical lattices, these dependencies will be retained. In other words, the unit cells near the z-axis of the optical lattice will have a lower intensity than the unit cells placed on a high-intensity area of the incident OV beam. Thus, absorbing particles trapped in unit cells at the center of an optical lattice will hardly leave it. It is expected that the 3D optical lattices with nonzero TCs will be tolerant to the perturbations induced by trapped particles, which rests upon the features of the Talbot effect.

For the more detailed consideration, **Figure 4** shows the experimental and calculated intensity profiles for different TCs of the incident beams at the specific Talbot planes together with the corresponding calculated phase profiles. It can be seen from these profiles that, when the incident beam passes through grating holes, pairs of discontinuities arise in its wave front, which results in the occurrence of singularities at the opposite ends of these discontinuities. The OVs occur around the phase singularities; the behavior of such singularities has been studied since.[28,29] It was found that, in free space, singularities appeared in such a way that the total TC remained unchanged; that is, in most cases, this means that the singularities with TCs of the opposite signs occur pairwise. In our case, two aspects were found to take place during propagation of the optical field. First, as the number of OV pairs decreases, their annihilation prevails over their creation. Second, as the optical field evolves, the optical singularities are spatially redistributed such that the OVs of the same total TC as that corresponding to the incident beam occur in the vicinity of the high-intensity areas, while the TCs of the opposite sign pass to the low-intensity area and, then, become indistinguishable. This yields a regular OV array in the far-field; each OV has a TC of the incident beam.

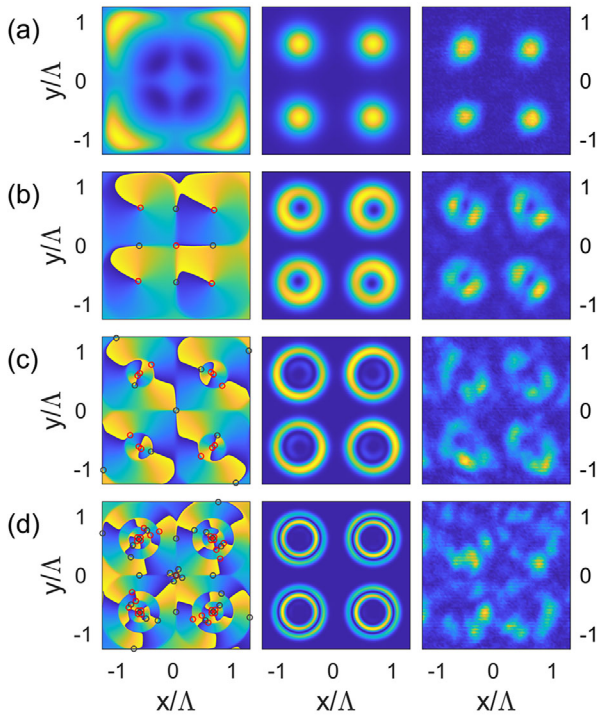

Figure 4. Calculated phase (left column) and intensity (middle column) profiles and experimental (right column) intensity profiles for specific sets {TC, TP} in rows: a) {0, 5}; b) {+1, 4}; c) {+2, 3}; d) {+3, 2}. Red and black circles show positions of the OVs with the positive and negative TCs.

The calculation showed that, at TC $l = +2$, the phase distribution is more complex, the second ring of the lower-intensity diffraction maxima appears inside the first one, and there are three rings for TC $l = +3$. Unfortunately, we failed experimentally resolve these rings by the reason of insufficient resolution of the beam profiler. It can be seen from Figure 4 that the vortices have a strongly asymmetric intensity distribution; moreover, it should be noted that the vortices located at different distances from the center are significantly different. However, these features are related to the incident beam size; in the limit case of a plane wave and an infinite grating, the individual vortices will not be different from each other and the radial intensity distribution will be more uniform.

In most cases, the OV propagating along the incident beam wavevector at $(x = 0, y = 0)$ has the same TC as the incident

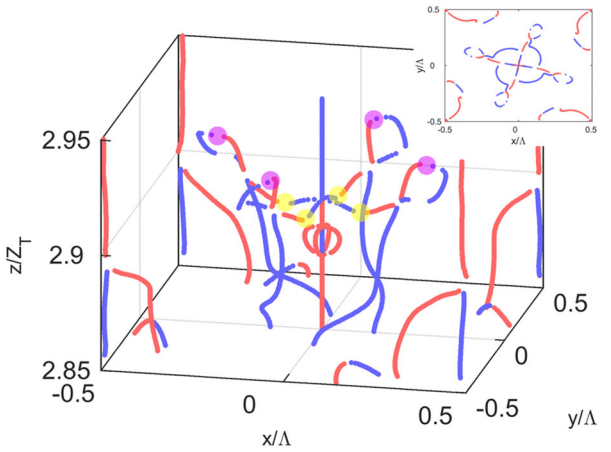

Figure 5. Trajectories of the OVs with the positive (red) and negative (blue) TC in the area restricted by the coordinates $z \in [2.85Z_T, 2.95Z_T]$ for the incident beam TC $l = +2$ (see visualization 1). Yellow and pink markers indicate the creation and annihilation points of OVs, respectively. Inset: the top view of OVs trajectories.

beam TC. Surprisingly, as can be seen in Figure 4c, a singularity with TC $l = -2$ appeared at the center of the phase profile at the third Talbot plane for the incident beam with $l = +2$. By this reason, the evolution of singularities for the incident beam with $l = +2$ from $z = 2.85Z_T$ to $z = 2.95Z_T$ was analyzed as shown in **Figure 5**. It was established that the TC of the central OV changes its sign during propagation. To be exact, the sign changes three times. First, at $z = 2.882Z_T$, the central vortex with TC $l = +2$ is divided into four vortices with TC $l = +1$ and the central vortex with TC $l = -2$. After that, at $z = 2.895Z_T$, these vortices are brought back together, which yields a single OV with TC $l = +2$. Then, at $z = 2.903Z_T$, four pairs of vortices with TC $l = \pm 1$ created at a certain distance from the center and the vortices with negative TCs move toward the center, while the positive ones run away from it. At $z = 2.906Z_T$, the trajectories of four vortices with TC $l = -1$ intersect with the central vortex with TC $l = +2$ at the center; as a result, at the center, a single vortex with TC $l = -2$ is formed (see visualization 1). This TC is preserved in the third Talbot plane. Nevertheless, the total TC across the lattice is kept the same as the TC of the incident beam during propagation.

4. Conclusion

We numerically predicted that the 3D optical lattices of optical vortices can be formed using the Talbot effect from Fresnel diffraction of light beams with a nonzero TC charge on a 2D regular transparency mask. These predictions were experimentally confirmed by the 3D optical vortex lattices reconstruction. Unfortunately, the spatial resolution of the beam profiler was not enough to resolve fine structure within the unit cells for high TC values. It was shown that the TC of the central singularity of the lattice alternates along the propagation direction. It was established that the optical vortices are created and annihilated during the propagation of light behind the mask in such a way that the total TC is preserved. The 3D OVLs with a nonzero TC are expected to be tolerant to the perturbations induced by trapped particles. 3D optical vortex lattices can ensure new functionalities for light-matter interactions, namely for transport and manipulation of multiple micro-object particles, which are impossible with the optical lattices without TCs.

Supporting Information

Supporting Information is available from the Wiley Online Library or from the author.

Acknowledgements

This work was supported by the Russian Science Foundation (Grant No. 19-12-00203).The surface grating was fabricated and characterized at the Center for Collective Use of the Krasnoyarsk Scientific Center, Siberian Branch, Russian Academy of Sciences. The authors thank M. N. Volochaev and A. I. Zaitsev for help.

Conflict of Interest

The authors declare no conflict of interest.

Data Availability Statement

Research data are not shared.

Keywords

optical lattices, optical vortices, Talbot effect

Received: March 12, 2021
Revised: April 23, 2021
Published online:

[1] M. J. Padgett, *Opt. Express* **2017**, *25*, 11265.
[2] Y. Shen, X. Wang, Z. Xie, C. Min, X. Fu, Q. Liu, M. Gong, X. Yuan, *Light: Sci. Appl.* **2019**, *8*, 90.
[3] M. Padgett, R. Bowman, *Nat. Photonics* **2011**, *5*, 343.
[4] V. G. Shvedov, A. S. Desyatnikov, A. V. Rode, Y. V. Izdebskaya, W. Z. Krolikowski, Y. S. Kivshar, *Appl. Phys. A* **2010**, *100*, 327.
[5] Y. Kozawa, D. Matsunaga, S. Sato, *Optica* **2018**, *5*, 86.
[6] Z. Yang, X. Lin, H. Zhang, Y. Xu, L. Jin, Y. Zou, X. Ma, *Optics and Lasers in Engineering* **2020**, *126*, 105899.
[7] V. G. Shvedov, C. Hnatovsky, A. V. Rode, W. Krolikowski, *Opt. Express* **2011**, *19*, 17350.
[8] J. Pu, M. Dong, T. Wang, *Appl. Opt.* **2006**, *45*, 7553.
[9] V. G. Shvedov, C. Hnatovsky, N. Shostka, A. V. Rode, W. Krolikowski, *Opt. Lett.* **2012**, *37*, 1934.
[10] J. Wang, J.-Y. Yang, I. M. Fazal, N. Ahmed, Y. Yan, H. Huang, Y. Ren, Y. Yue, S. Dolinar, M. Tur, A. E. Willner, *Nat. Photonics* **2012**, *6*, 488.
[11] N. Bozinovic, Y. Yue, Y. Ren, M. Tur, P. Kristensen, H. Huang, A. E. Willner, S. Ramachandran, *Science* **2013**, *340*, 1545.
[12] G.-X. Wei, L.-L. Lu, C.-S. Guo, *Opt. Commun.* **2009**, *282*, 2665.
[13] H. Rubinsztein-Dunlop, A. Forbes, M. V. Berry, M. R. Dennis, D. L. Andrews, M. Mansuripur, C. Denz, C. Alpmann, P. Banzer, T. Bauer, E. Karimi, L. Marrucci, M. Padgett, M. Ritsch-Marte, N. M. Litchinitser, N. P. Bigelow, C. Rosales-Guzmán, A. Belmonte, J. P. Torres, T. W. Neely, M. Baker, R. Gordon, A. B. Stilgoe, J. Romero, A. G. White, R. Fickler, A. E. Willner, G. Xie, B. McMorran, A. M. Weiner, *J. Opt.* **2016**, *19*, 013001.

[14] C.-S. Guo, Y.-N. Yu, Z. Hong, *Opt. Commun.* **2010**, *283*, 1889.
[15] W. Li, M. C. Marconi, *Opt. Express* **2015**, *23*, 25532.
[16] P. J. P. Chausse, E. D. L. Boulbar, S. D. Lis, P. A. Shields, *Opt. Express* **2019**, *27*, 5918.
[17] S. Schwarz, C. Kapahi, R. Xu, A. R. Cameron, D. Sarenac, J. P. W. MacLean, K. B. Kuntz, D. G. Cory, T. Jennewein, K. J. Resch, D. A. Pushin, *Phys. Rev. A: At., Mol., Opt. Phys.* **2020**, *101*, 043815.
[18] J. Becker, P. Rose, M. Boguslawski, C. Denz, *Opt. Express* **2011**, *19*, 9848.
[19] A. Kelberer, M. Boguslawski, P. Rose, C. Denz, *Opt. Lett.* **2012**, *37*, 5009.
[20] J. Yu, C. Zhou, W. Jia, A. Hu, W. Cao, J. Wu, S. Wang, *Appl. Opt.* **2012**, *51*, 2485.
[21] B. Knyazev, O. Kameshkov, N. Vinokurov, V. Cherkassky, Y. Choporova, V. Pavelyev, *Opt. Express* **2018**, *26*, 14174.
[22] X. Li, H. Ma, H. Zhang, Y. Tai, H. Li, M. Tang, J. Wang, J. Tang, Y. Cai, *Opt. Express* **2018**, *26*, 22965.
[23] I. A. Kotelnikov, O. E. Kameshkov, B. A. Knyazev, *J. Opt.* **2020**, *22*, 065603.
[24] D. A. Ikonnikov, S. A. Myslivets, M. N. Volochaev, V. G. Arkhipkin, A. M. Vyunishev, *Sci. Rep.* **2020**, *10*, 20315.
[25] P. Rose, M. Boguslawski, C. Denz, *New J. Phys.* **2012**, *14*, 033018.
[26] J. Wen, Y. Zhang, M. Xiao, *Adv. Opt. Photon.* **2013**, *5*, 83.
[27] P. Zemánek, G. Volpe, A. Jonáš, O. Brzobohatý, *Adv. Opt. Photon.* **2019**, *11*, 577.
[28] J. F. Nye, M. V. Berry, *Proc. R. Soc. London, Ser. A* **1974**, *336*, 165.
[29] I. Freund, N. Shvartsman, *Phys. Rev. A* **1994**, *50*, 5164.